Japanese Journal of Applied Physics

The Japan Society of Applied Physics

REGULAR PAPER

Transverse energy confinement and resonance suppression in SAW resonators using low-cut lithium tantalate

To cite this article: Yiwen He *et al* 2022 *Jpn. J. Appl. Phys.* **61** SG1031

Japanese Journal of Applied Physics **61**, SG1031 (2022) **REGULAR PAPER**
https://doi.org/10.35848/1347-4065/ac4821

Transverse energy confinement and resonance suppression in SAW resonators using low-cut lithium tantalate

Yiwen He[1], Yu-Po Wong[2], Qi Liang[1], Ting Wu[1], Jingfu Bao[1*], and Ken-ya Hashimoto[1,2]

[1]*School of Electronic Science and Engineering, University of Electronic Science and Technology of China, Chengdu 611731, People's Republic of China*
[2]*Graduate School of Engineering, Chiba University, Chiba 263-8522, Japan*

[*]E-mail: baojingfu@uestc.edu.cn

Received October 26, 2021; revised December 23, 2021; accepted January 4, 2022; published online April 29, 2022

This paper discusses the applicability of double busbar design to surface acoustic wave (SAW) devices employing low-cut lithium tantalate (LT) with a multi-layered structure. This design offers good energy confinement, scattering loss suppression and transverse mode suppression for a wide frequency range. In addition, the effectiveness of manipulating the slowness curve shape for transverse mode suppression is demonstrated. First, three different lateral edge designs are applied to the layered SAW configuration on low-cut LT, and their performances are compared using the periodic three-dimensional finite-element method powered by the hierarchical cascading technique. Then, the discussion is extended to the influence of the SAW slowness shape to the transverse mode suppression.

1. Introduction

Recently, surface acoustic wave (SAW) resonators employing multi-layered structures, such as incredible high performance (I.H.P.) SAW, have aroused appreciable interest owing to its small temperature coefficient of frequency and high quality factors (Q) owing to excellent acoustic energy confinement.[1–17] Despite the fact that energy can be well confined to the surface, there still remains lateral energy leakage through the busbar which causes excess loss. For its ultimate reduction, lateral edges including busbars and gaps between electrode finger tips must be designed properly.

It is known that dummy electrodes (dummies) are necessary to suppress scattering loss when the rotation angle θ of $LiTaO_3$ (LT) substrate is chosen at about 42°, namely 42-LT.[18] However, they weaken the lateral energy confinement, and energy leakage occurs.[19] Huck et al. proposed to use the gap short structure,[20] instead of dummies, for further suppression.

This year, the authors' group proposed[19] the double busbar configuration with piston mode design,[21,22] which offers both good energy confinement and transverse mode suppression for layered SAW structures employing 42-LT such as I.H.P. SAW.

Layered structures using LT with small θ,[23] for example, 20°, also seem promising for achieving larger electromechanical coupling factor (k^2) than 42-LT.[13] The authors attempted to apply the double busbar configuration to the layered structure using 20-LT.[24] Although well energy confinement was achieved, transverse mode resonances could not be well suppressed. The authors thought this is due to convex shape of the SAW slowness curve on the 20-LT plate. In contrast, the slowness shape is concave for shear-horizontal (SH) SAWs on 42-LT itself, and the curvature can be adjusted by the layer design.[25]

This paper is the extended version of Ref. 24, and discusses applicability of the double busbar configuration to multi-layered SAW resonators on low-cut LT for better energy confinement and spurious resonance suppression. Influence of the slowness curve shape is also studied for the transverse mode suppression.

First, three different lateral edge designs are applied to the layered SAW configuration on 20-LT, and their performances are compared. The analysis is performed by the periodic three dimensional (3D) finite element method (FEM) powered by the hierarchical cascading technique.[26–31] It is shown that the double busbar configuration offers good energy confinement in addition to suppression of transverse mode resonances in some extent.

Then, the discussion is extended to influence of the SAW slowness shape to the transverse mode suppression. The influence is enormous, and transverse resonances can be suppressed well when the slowness shape is almost flat. Note that the flat slowness shape is realizable by reducing the electrode thickness even when θ is small although it reduces k^2.

2. Double busbar design on 20-LT plate

2.1. Comparison of three different lateral edge designs

Figure 1(a) shows one period of the 20-LT/SiO_2/Si structure discussed in this paper. Figures 1(b)–1(d) show one period of the electrode patterns discussed in this paper: (b) and (c) are the conventional ones without and with dummy electrodes, respectively, while (d) is the double-busbar structure proposed by the authors.[24] The perfect matching layers (PMLs) are given to the side edges, while the periodic boundary conditions are applied to the top and bottom boundaries. Since only tiny material loss is added in the FEM model, losses appearing in the following analyses are mainly due to energy leakage through busbars and scattering to bulk waves. In the following calculation, used parameters are taken from authors' previous work using 42-LT[24] and given in Table I.

Figure 2 shows admittance (Y) and conductance (G) calculated by periodic 3D FEM. When the dummies are not given, the conductance levels are elevated upward at frequencies above 1.925 GHz [see Fig. 2(a)]. This is caused by the scattering at the gap region.[18,19] Figure 3(a) shows the field distribution of the "without dummies" design at 1.944 GHz. The red lines are the outline of electrodes and busbar region. Energy concentration is seen near the gap region which is responsible for the scattering loss.

On the other hand, when the dummies are given, the elevation was suppressed [see Fig. 2(b)]. Note that shorter gap length gives better performance as well as cases using 42-LT;[18] both electrical and mechanical effects of dummies are responsible for the scattering reduction. Spurious

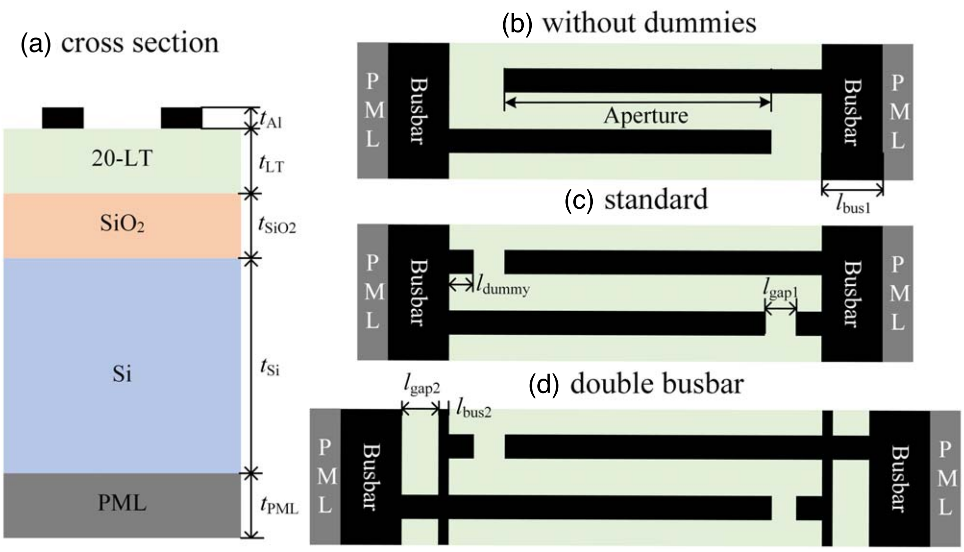

Fig. 1. (Color online) Unit cells of three designs of the multi-layered SAW on 20-LT: (a) cross section, (b) standard design without dummy electrodes, (c) standard design with dummy electrodes, and (d) double busbar design.[24)]

Table I. Simulation parameters.

Parameters	Value
Piezoelectric material	20-LT
Electrode material	Aluminum
IDT period (p_I)	2 μm
Electrode layer thickness (t_{Al})	0.09 p_I
Piezoelectric layer thickness (t_{LT})	0.368 p_I
Silicon dioxide layer thickness (t_{SiO2})	0.3 p_I
Silicon layer thickness (t_{Si})	1.5 p_I
PML layer (t_{PML})	1 p_I
Metallization ratio (MR)	0.35
Aperture	12.8 p_I
Gap length (l_{gap1})	0.2 p_I
Busbar length (l_{bus1})	6.85 p_I
Dummy electrode length (l_{dummy})	0.9 p_I
Secondary gap length (l_{gap2})	0.9 p_I
Secondary busbar length (l_{bus2})	0.3 p_I

resonance peaks are not steep above 1.925 GHz. Figure 3(b) shows the field distribution of the "standard" design at 1.95 GHz. Although the energy concentration does not occur in this case, energy leakage to the busbar region is clearly seen. Namely, the transverse modes are leaky in this frequency range.

In contrast, when the double busbar is applied, resonance peaks keep steep until 1.965 GHz. The extra gap region has higher acoustic velocity, so it can act as an energy barrier. Thus, the energy is mainly trapped within the aperture region. This further indicates that even on the low-cut LT, the double busbar configuration can provide better lateral energy confinement for wider frequency range. Although larger l_{gap2} can further enhance the lateral leakage suppression, it can also lead to larger ohmic resistance. As a compromise, l_{gap2} is set to 0.9 p_I.

Note that some energy leakage can still be seen above 1.965 GHz. This is due to insufficient SAW velocity difference between electrode and gap regions.[19)] This problem might be solved by redesigning the whole device configuration.

2.2. Piston mode operation on double busbar structure

Although double busbar can provide good energy confinement, some transverse resonances still remain in the passband

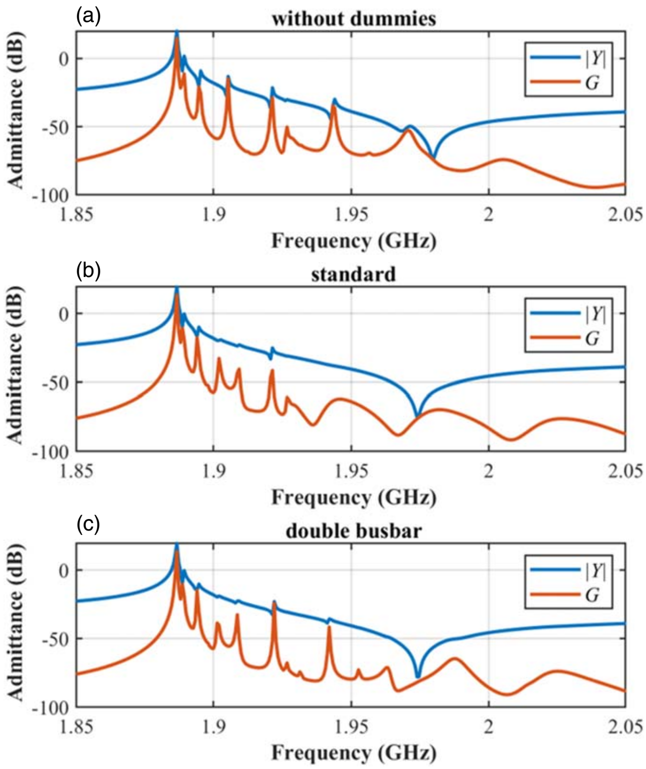

Fig. 2. (Color online) Calculated Y and G: (a) standard design without dummies design, (b) standard design, and (c) double busbar design.[24)]

[see Fig. 2(c)]. Then, the piston mode is applied to the double busbar structure for further transverse mode suppression. The inset of Fig. 4(a) shows the electrode configuration including optimized "hammer heads"[21,22)] for the piston mode operation.

Figure 4(a) shows change of Y and G of double busbar design with the piston mode design. The effect of piston mode operation is significant. Transverse modes are suppressed in some extent. This can also be seen from the comparison of Bode Q[32)] curve in Fig. 4(b). The notches in the blue curve from 1.9 GHz to 1.95 GHz become smaller which also confirms the good impact of piston mode

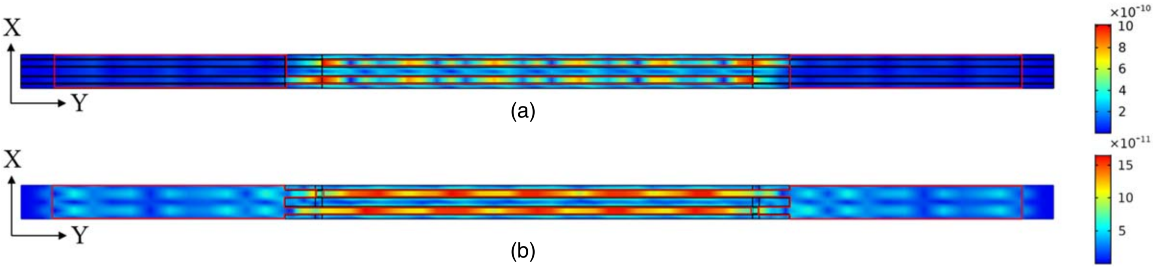

Fig. 3. (Color online) Field distribution of (a) without dummies design at 1.944 GHz, and (b) standard design at 1.95 GHz. Note that the color scale for (b) is 0.15 times smaller than that for (a).

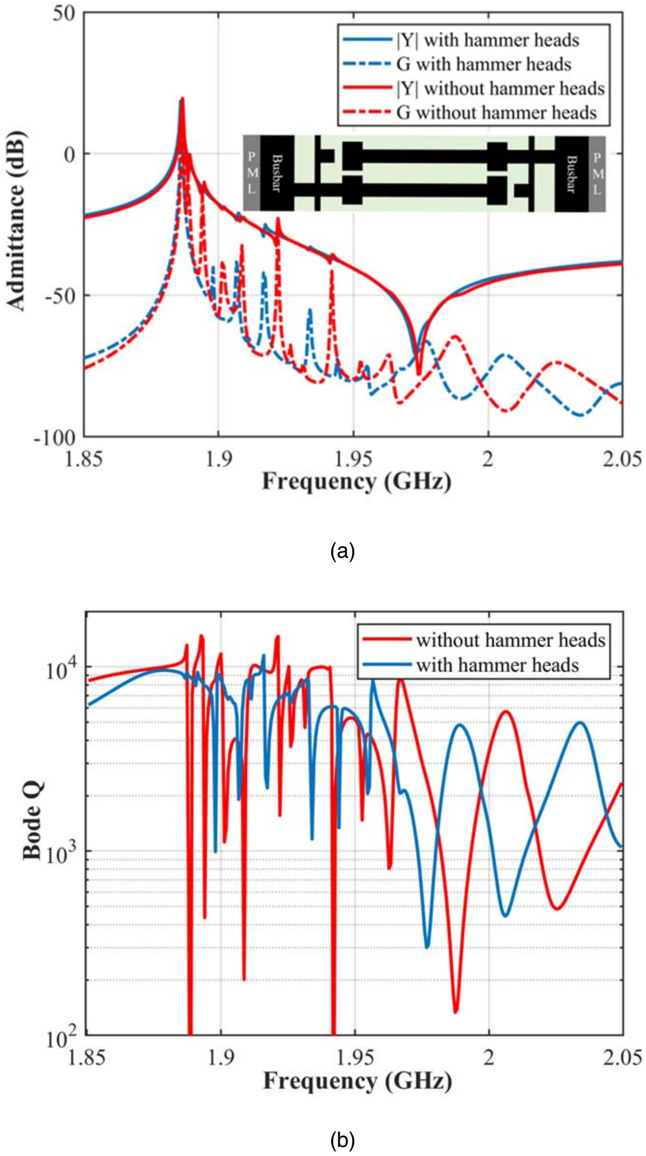

Fig. 4. (Color online) Variation of Y, G and Bode Q when the hammer heads are given.[24]

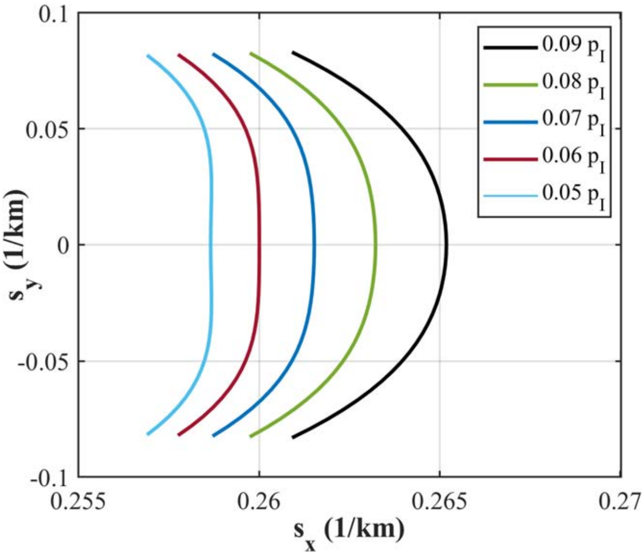

Fig. 5. (Color online) Variation of slowness shape with t_{Al} when 20-LT is employed.

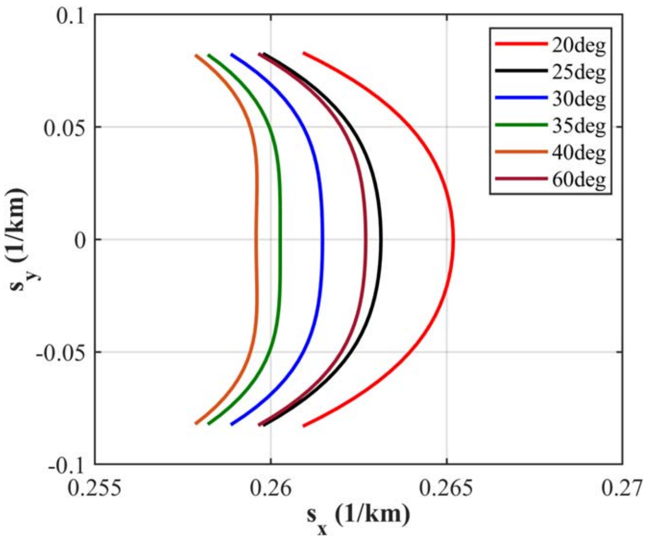

Fig. 6. (Color online) Variation of slowness shape with θ when $t_{\mathrm{Al}} = 0.09\ p_{\mathrm{I}}$.

operation. No apparent degradation is seen by the application of "hammer heads".

3. Influence of slowness shape to transverse mode suppression

The spurious suppression of this result is inferior to that obtained when 42-LT was used instead of 20-LT.[19] Namely, there still remain several spurious resonances hard to eliminate by the "hammer heads" design. This is expected to be related to the slowness curve shape of the SH SAW under concern. Note that the slowness shape can be quite flat near the crystal X direction when 42-LT is employed.[2,3,25]

It is known that the slowness shape can be adjusted effectively by tuning the metallization ratio (MR), rotation angle θ, t_{LT}, t_{SiO2}, and t_{Al} for SAW structure.[25] Among these parameters, slowness shape is most sensitive to t_{Al}.

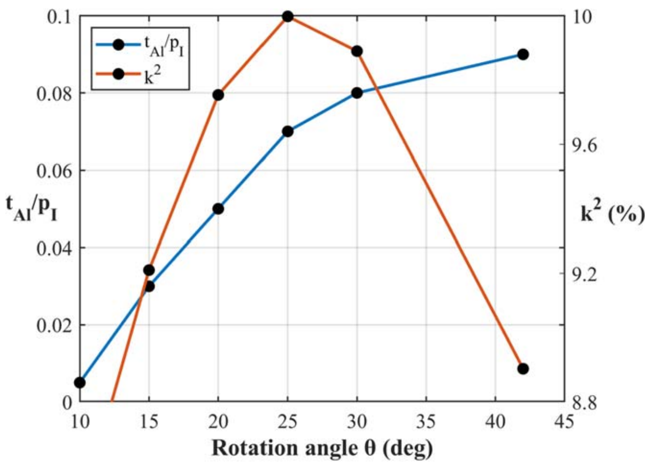

Fig. 7. (Color online) Variation of t_{Al} giving the flat slowness and k^2 at the setting with θ.

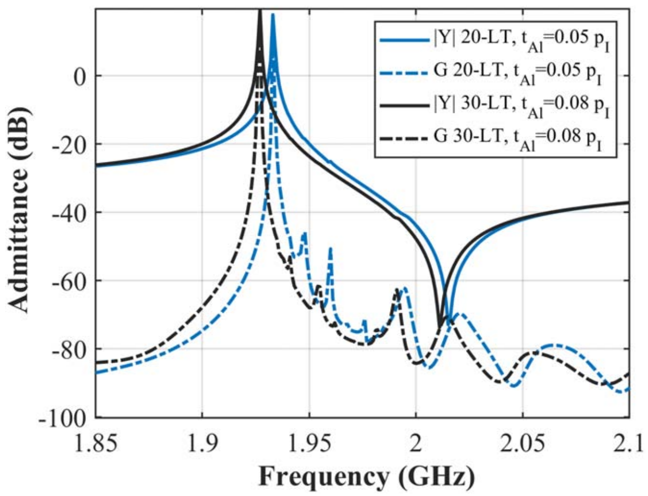

Fig. 8. (Color online) Calculated Y and G when the hammer heads are given and θ and t_{Al} are set to give the flat slowness shape.

Figure 5 shows how the slowness shape in the aperture region changes with t_{Al} when 20-LT is used. The flat slowness shape can be achieved when t_{Al} is set to 0.05 p_I. Figure 6 shows how the slowness shape changes with θ when t_{Al} is fixed to 0.09 p_I. In this case, the flat slowness shape appears when θ is close to 42°.

Figure 7 shows that how t_{Al} giving the flat slowness changes with θ. It is seen that the flat slowness shape is achievable by reducing t_{Al} even when θ is small.

Then, periodic 3D FEM simulations are carried out to for the cases: (a) 20-LT is chosen and t_{Al} is set at 0.05 p_I, and (b) 30-LT is chosen and t_{Al} is set at 0.08 p_I. In these settings, the slowness curves are mostly flat.

Figure 8 shows calculated Y and G. Transverse modes are well suppressed between resonance and anti-resonance frequencies for both cases. This indicates that even low-cut LT is chosen as the piezoelectric layer, better transverse mode suppression can also be achieved by manipulating the slowness shape. And near flat slowness shape is preferable to realize almost complete transverse mode suppression.

By the way, it is known that reduction of t_{Al} causes that of k^2 in these substrates.[33] Figure 7 also shows how estimated k^2 under the flat slowness condition changes with θ. Due to the t_{Al} reduction, increase of k^2 is quite limited even when θ is small. Namely, although k^2 takes a maximum at $\theta \sim 25°$, its increment from 42-LT is limited to about 1%.

4. Conclusion

This paper discussed the applicability of double busbar design to multi-layered SAW devices employing low-cut LT for better lateral energy confinement and spurious resonance suppression. Influence of the slowness curve shape was also studied for the transverse mode suppression.

First, it was shown that dummies are necessary for scattering suppression in 20-LT and a narrow gap is preferable, as well as cases using 42-LT. Besides, double busbar can provide wider energy confinement while realize the electrode connection for dummies to create an extra gap between dummies and busbar. It was also shown that transverse modes can be suppressed in some extent by applying the hammer heads onto double busbar configuration.

Then the discussion was extended to the influence of slowness shape to transverse mode suppression. It was indicated that even low-cut LT is chosen as the piezoelectric layer, better transverse mode suppression can also be realizable by manipulating the slowness shape in the trade-off with achievable k^2.

Acknowledgments

This work was supported in part by the Research Project under Grant A1098531023601318 and in part by the National Natural Science Foundation of China and the China Academy of Engineering Physics under Grant U1430102.

ORCID iDs

Yiwen He https://orcid.org/0000-0003-3930-6026
Yu-Po Wong https://orcid.org/0000-0003-4372-2786
Ting Wu https://orcid.org/0000-0003-0070-756X

1) T. Takai et al., Proc. IEEE Ultrason. Symp., 2016, 10.1109/ULTSYM.2016.7728455.
2) T. Takai et al., IEEE Trans. Ultrason., Ferroelectr. Freq. Control **64**, 1382 (2017).
3) H. Iwamoto, T. Takai, Y. Takamine, T. Nakao, T. Fuyutsume, and M. Koshino, Proc. IEEE Ultrason. Symp., 2018, 10.1109/ULTSYM.2018.8580175.
4) T. Takai, H. Iwamoto, Y. Takamine, T. Fuyutsume, T. Nakao, M. Hiramoto, T. Toi, and M. Koshino, IEEE Trans. Ultrason. Ferroelectr. Freq. Control **66**, 1006 (2019).
5) T. Kimura, M. Omura, Y. Kishimoto, and K. Hashimoto, IEEE Trans. Microwave Theory Tech. **67**, 915 (2019).
6) T. Kimura, Y. Kishimoto, M. Omura, and K. Hashimoto, Jpn. J. Appl. Phys. **57**, 07LD15 (2018).
7) N. Matsuoka, T. Omori, and K. Hashimoto, Proc. IEEE Ultrason. Symp., 2019, 10.1109/ULTSYM.2019.8926253.
8) Z. Wu, K. Gong, Y. P. Wong, J. Bao, and K. Hashimoto, Proc. IEEE Ultrason. Symp., 2021, 10.1109/IUS52206.2021.9593373.
9) S. Inoue and M. Solal, Proc. IEEE Ultrason. Symp., 2018, 10.1109/ULTSYM.2018.8579852.
10) S. Inoue and M. Solal, Proc. IEEE Ultrason. Symp., 2020, 10.1109/IUS46767.2020.9251459.
11) M. Kadota and S. Tanaka, Jpn. J. Appl. Phys. **57**, 07LD12 (2018).
12) M. Kadota, Y. Ishii, and S. Tanaka, Jpn. J. Appl. Phys. **59**, SKKC11 (2020).
13) M. Kadota, Y. Ishii, and S. Tanaka, IEEE Trans. Ultrason., Ferroelectr. Freq. Control **68**, 1955 (2021).
14) M. Gomi, T. Kataoka, J. Hayashi, and S. Kakio, Jpn. J. Appl. Phys. **56**, 07JD13 (2017).

15) J. Hayashi, K. Yamaya, M. Suzuki, S. Kakio, H. Suzaki, T. Yonai, K. Kishida, and J. Mizuno, Jpn. J. Appl. Phys. **57**, 07LD21 (2018).
16) S. Kakio, Jpn. J. Appl. Phys. **60**, SD0802 (2021).
17) N. F. Naumenko, IEEE Trans. Ultrason. Ferroelectr. Freq. Control **67**, 1485 (2020).
18) M. Solal, L. Chen, and J. Gratier, IEEE Trans. Ultrason., Ferroelectr. Freq. Control **60**, 2404 (2013).
19) Y. P. Wong, Y. He, N. Matsuoka, Q. Liang, J. Bao, and K. Hashimoto, Proc. IEEE Ultrason. Symp., 2021, 10.1109/IUS52206.2021.9593517.
20) C. Huck, International Patent WO 2020/120153 (2020).
21) M. Solal, J. Gratier, R. Aigner, K. Gamble, B. Abbott, T. Kook, A. Chen, and K. Steiner, Proc. IEEE Ultrason. Symp., 2010, p. 624, 10.1109/ULTSYM.2010.5935738.
22) M. Solal, J. Gratier, R. Aigner, and K. Gamble, U.S. Patent 7939989 B2 (2011).
23) K. Hashimoto, "6.3.3. LiTaO3," *Surface Acoustic Wave Devices in Telecommunications* (Springer, Hidelberg, 2000), p. 179.
24) Y. He, Y. P. Wong, Q. Liang, T. Wu, J. Bao, and K. Hashimoto, Proc. Symp. Ultrason. Electron, 2021, 2Pa3-1.
25) Y. P. Wong, N. Matsuoka, L. Qiu, and K. Hashimoto, Proc. IEEE Ultrason. Symp., 2020, 10.1109/IUS46767.2020.9251446.
26) J. Koskela, P. Maniadis, B. A. Willemsen, P. J. Turner, R. B. Hammond, N. O. Fenzi, and V. Plessky, Proc. IEEE Ultrason. Symp., 2016, 10.1109/ULTSYM.2016.7728574.
27) V. Plessky, J. Koskela, B. A. Willemsen, P. J. Turner, F. Iliev, R. B. Hammond, and N. O. Fenzi, Proc. IEEE Ultrason. Symp., 2017, 10.1109/ULTSYM.2017.8091824.
28) J. Koskela, V. Plessky, B. Willemsen, P. Turner, B. Hammond, and N. Fenzi, IEEE Trans. Ultrason., Ferroelectr. Freq. Control **65**, 1933 (2018).
29) X. Li, J. Bao, Y. Huang, B. Zhang, T. Omori, and K. Hashimoto, Jpn. J. Appl. Phys. **57**, 07LC08 (2018).
30) X. Li, J. Bao, Y. Huang, B. Zhang, T. Omori, and K. Hashimoto, IEEE Trans. Ultrason., Ferroelectr. Freq. Control **66**, 1920 (2019).
31) K. Hashimoto, Y. P. Wong, N. Matsuoka, X. Li, Y. Huang, and J. Bao, Proc. IEEE Ultrason. Symp., 2021, 10.1109/IUS52206.2021.9593481.
32) D. A. Feld, R. Parker, R. Ruby, P. Bradley, and S. Dong, Proc. IEEE Ultrason. Symp., 2008, p. 431, 10.1109/ULTSYM.2008.0105.
33) K. Hashimoto and M. Yamaguchi, Proc. IEEE Ultrason. Symp., 1996, p. 117, 10.1109/ULTSYM.1996.583819.